Open Archive Toulouse Archive Ouverte (OATAO)

To cite this version:

Audigié, Pauline and Vande Put, Aurélie and Malié, André and Monceau, Daniel *High-temperature cyclic oxidation behaviour of Pt-rich γ-γ' coatings. Part I: Oxidation kinetics of coated AM1 systems after very long-term exposure at 1100 °C.* (2018) Corrosion Science, 144. 127-135. ISSN 0010-938X

High-temperature cyclic oxidation behaviour of Pt-rich γ-γ' coatings. Part I: Oxidation kinetics of coated AM1 systems after very long-term exposure at 1100 °C

Pauline Audigié[a],[*], Aurélie Rouaix-Vande Put[a], André Malié[b], Daniel Monceau[a]

[a] *CIRIMAT, University of Toulouse, ENSIACET, 4 Allée Emile Monso, BP 44362, 31030, Toulouse Cedex 4, France*
[b] *SAFRAN AIRCRAFT ENGINE, 99 rue Maryse Bastié, BP 129, 86101 Châtellerault Cedex, France*

ARTICLE INFO

ABSTRACT

The cyclic oxidation behaviour of several compositions of Pt-rich γ-γ' bond-coatings on AM1 superalloy was studied at 1100 °C and was compared to the β-(Ni,Pt)Al coated and uncoated superalloy. AM1 superalloy exhibited an outstanding performance due to an optimized Hf doping and a low sulfur content. The Pt-rich γ-γ' bond-coatings showed a better cyclic oxidation resistance than the reference system with a β-(Ni,Pt)Al coating. Aluminium addition during fabrication was found to be beneficial to improve the oxidation behaviour of Pt-rich γ-γ' bond-coatings. Their breakaway resulted from an insufficient aluminium content below the TGO whereas the reference system suffered from rumpling.

1. Introduction

Improving aircraft engine efficiency and reducing fuel consumption, atmospheric emissions and noisiness still constitutes a great challenge for aircraft designers. In that respect, emphasis has been placed for many years upon reducing the weight of the overall structure as well as improving gas-turbine performances. This led to progressively increase the gas inlet temperatures, subjecting the high-pressure turbine parts like blades and vanes to more severe conditions. In order to resist against excessive oxidation and to lower the temperature at the component surface, the multi-layered Thermal Barrier Coating (TBC) system was developed. Current TBC systems are composed of a ceramic outer layer of 6–8 wt.% yttria partially stabilized zirconia (YSZ) and a bond-coating deposited on a nickel-based superalloy. MCrAlY overlay (where M = Ni, Co or both) or platinum-modified diffusion aluminide (β-(Ni,Pt)Al) were selected as bond-coatings for their high aluminium content necessary to sustain the growth of the thermally grown oxide (TGO), an α-alumina scale.

However, a number of previous papers reports the significant improvement of TBC lifetime provided by Pt-rich γ-γ' bond-coatings. They were originally studied for their corrosion and oxidation resistance, their good mechanical compatibility with the superalloy and as a lower cost alternative to β-(Ni,Pt)Al coatings [1–5]. Nevertheless, their higher sensitivity to the substrate [6–9] and particularly their lower aluminium reservoir alter selective aluminium oxidation over long service durations. Two main ideas were developed in order to bypass these critical elements. Reactive element addition was used to slow down the oxidation kinetics [10,11] and to reduce carbon and sulphur segregations at the metal/oxide interface in order to reduce oxide scale spallation [12,13]. But the main improvement in the oxidation behaviour was by the addition of platinum. Platinum allows the uphill aluminium diffusion from the bulk to the surface [14–16], improves the adhesion of the oxide scale [14,17–19] by reducing sulphur segregation at the metal/oxide interface [17,19] or by avoiding the formation of Kirkendall voids at the same interface [20–22]. In addition, platinum brings to the Pt-rich γ-γ' coatings the capacity to form an alumina scale. By segregating at the (100), (110) and (111) free surfaces in the nickel lattice of the γ' phase, platinum increases the Al:Ni ratio at the surface [23–25]. Consequently, for a given aluminium concentration, the activity of nickel is reduced which favours alumina formation [24]. In platinum-rich γ phase, alumina formation occurs with only 10 at.% of aluminium versus 32 at.% in a Ni-Al binary alloy [26].

In a previous study [27], two compositions of Pt-rich γ-γ' bond-coatings offering good oxidation resistance were identified. These bond-coatings were fabricated by spark plasma sintering (SPS) from platinum and aluminium foil stacking as it is a relevant tool to fabricate coatings and complete TBC systems in a short duration [28]. The Ni-30 Pt-25Al (at.%) platinum-rich composition was obtained from a 5 μm thick platinum foil and a 2 μm thick aluminium foil while the Ni-28Al-17Pt (at. %) aluminium-rich composition was obtained from platinum and

aluminium foils of 5 μm thick each. A first objective of this study was to obtain these bond-coating compositions from conventional industrial processes. In the literature, the Pt-rich γ-γ' coatings were mainly prepared by diffusion of an electroplated platinum layer deposited on a nickel-based superalloy. Therefore, they were named "Pt-only γ-γ' coatings". In this study, in order to identify if aluminium addition during fabrication can have an effect on the oxidation performance, a few systems were fabricated from a platinum electroplating followed by an annealing and a short-term aluminizing step. These coatings were referenced as Pt + Al γ-γ'. For comparison, Pt-rich γ-γ' coatings as well as Pt-modified β-NiAl coatings were made. The cyclic oxidation of these three systems was also compared to the behaviour of the uncoated Ni-based superalloy, AM1.

Although the Pt-rich γ-γ' coatings have been studied for more than twenty years, tests of cyclic oxidation resistance of more than 1000-1 h cycles at 1100 °C are infrequent. In order to quantify the lifetime increase brought by these coatings, a long-term cyclic oxidation test was performed over more than 15,000 cycles.

The first part of this study was focused on the assessment of the cyclic oxidation kinetics based on the results of the long-term cyclic oxidation test. Characterization of oxidized systems was then made to analyse the influence of platinum and aluminium contents in the bond-coating on the cyclic oxidation resistance. Performance of complete TBC systems with these bond-coatings, spallation kinetics as well as the effect of the coating composition will be discussed in a second publication.

2. Materials and experiments

The optimized composition of the AM1 first-generation single-crystal superalloy was used as a substrate. As it can be seen from its composition Ni-12Al-9Cr-7Co-2Ti-3Ta-2W-1Mo (at.%), with 0.12S-570Hf-25Zr-23C (ppmw), it was doped in hafnium and contained a low sulphur content.

Three kinds of bond-coatings were studied: Pt-only γ-γ', Pt + Al γ-γ' and β-(Ni,Pt)Al. All coatings were fabricated onto cylindrical AM1 samples (40 mm height x 8 mm diameter) which were grit-blasted with α-Al$_2$O$_3$ particles before deposition. Three samples of Pt-only γ-γ' coatings were prepared by electroplating 5 ± 2 μm of Pt followed by an annealing for 1 h in vacuum at 1100 °C. Three variants of Pt + Al γ-γ' coatings were prepared from different platinum and aluminium additions. A total of eleven systems with Pt + Al γ-γ' coatings were obtained from either 5 ± 2 μm or 7 ± 2 μm electroplated platinum, a heat treatment for 1 h under vacuum at 1100 °C and a "short-term" aluminizing. This latter corresponds to an interrupted vapour phase aluminizing process. Parameters such as the activator quantity or the dwell time at high temperature were adjusted in order to deposit either 5 μm or 2 μm of aluminium as reported in [29]. "Short-term" aluminizing is referenced in the Table 1 as aluminizing # 1, # 2 and # 3. The Pt + Al γ-γ' coatings were then named with their platinum/aluminium equivalent thicknesses in order to compare with the composition obtained by SPS from platinum and aluminium foil stackings. Equivalent thicknesses were calculating from the mass gains obtained after electroplating and aluminizing by considering that the deposits were fully dense. Therefore, the Pt + Al γ-γ' coatings were designated as 5/2, 5/5 and 7/5 compositions.

For comparison, three conventional systems with β-(Ni,Pt)Al coatings were fabricated from a 5 ± 2 μm thick Pt electroplated layer, a diffusion heat treatment for 1 h under vacuum at 1100 °C and a conventional vapour phase aluminizing (APVS). In addition, three samples of uncoated superalloy were also tested, two in the as-received condition and one polished up to grade P1200 with SiC. Sample designation and conditions of bond-coating fabrication are detailed in the Table 1. One sample of each system was defined as a reference in order to characterize the microstructure after 1 cycle of 1 h at 1100 °C.

Cyclic oxidation tests were performed under laboratory air on all

systems. The samples experienced a 1 h dwell at 1100 °C and cooling by forced convection during 15 min. Specimen mass changes were measured every 20–50 cycles until 750 cycles and every 150-200 cycles until the end-of-life using a Sartorius microbalance with an accuracy of ± 0.02 mg. The lifetime criteria was set to a specimen mass change of - 20 mg/cm². This corresponds to the loss of more than three times the aluminium quantity added to fabricate the β-(Ni,Pt)Al coating or more than ten times the one added for the Pt + Al γ-γ' coatings. Two or three samples per system were oxidized. After 3000, 5500, 10,000 cycles and at the end-of-life if reached, samples were removed from the oxidation rig to be characterized. Surfaces and cross-sections were characterized by scanning electron microscopy (SEM) and energy dispersive spectroscopy (EDS) using real standards for quantification. X-ray diffraction analysis (XRD), Raman spectroscopy and fluorescence were also conducted at different durations in order to determine the nature of the oxide scale and its evolution with time.

3. Results

3.1. As-fabricated coatings

Fig. 1 shows the backscattered electron images of metallographic cross-sections of each coating in the as-annealed state and Table 2 lists the layer thicknesses of these latter coatings. Residual alumina particles from grit-blasting appeared in black on the images marked the original superalloy surface.

The microstructure of the Pt-only γ-γ' coating (Fig. 1a) consisted of two distinct layers. The outer layer was mainly composed of a Pt-rich γ phase characterized by a lattice parameter equal to 0.3663 nm. The interdiffusion zone contained γ and γ' phases. Average concentrations were determined based on EDS analyses. 7.3 at.% of aluminium and 15.7 at.% of platinum were detected in the outer Pt-rich γ layer while 15.0 at.% of aluminium and 19.6 at.% of platinum were measured in the γ-γ' interdiffusion zone. Some voids were observed at the inter-diffusion zone/substrate interface. α-alumina scale was detected by fluorescence analysis at the coating surface. This thin oxide scale could have formed during the two hours exposure at 1100 °C, i.e. during the 1 h platinum diffusion heat treatment under vacuum and most likely during the 1 h air annealing. Neither transition alumina nor spinel were identified.

Fig. 1(b, c, d) exhibits the microstructure of the three variants of Pt + Al γ-γ' bond-coating. The coating thickness of the 5/2 composition was 27.2 ± 2.3 μm (Fig. 1b). The Pt-rich γ phase was found at the equilibrium with the Pt-rich γ' precipitates in the outer layer while a two-phased γ-γ' layer was observed below the grit-blasting particles. The coating thickness of the 5/5 composition, 28.8 ± 2.4 μm, was similar to the one of the 5/2 composition (Fig. 1c). However, the microstructure was different. A very thin layer of α-NiPtAl was formed at the subsurface due to a higher quantity of aluminium. Then, the intermediate layer consisted of a Pt-rich single phase γ' and the inner interdiffusion zone included coarse γ' particles in a γ-matrix. The average chemical compositions of the Pt-rich γ-γ' layers of the 5/2 and 5/5 compositions revealed a higher aluminium content in the aluminium-rich composition than expected (Table 3). Higher chromium and cobalt contents were detected in the platinum-rich composition when compared with the aluminium-rich composition.

In addition, less aluminium than expected was deposited with the aluminizing #2. Then further samples with 7 μm of platinum (against 5 μm previously) and around 5 μm of aluminium (7/5) were prepared from the aluminizing #3; they were defined as 7/5 composition. The microstructure of this coating in the as-annealed condition can be divided into three zones (Fig. 1d), two above the grit-blasting particles and one below. According to SEM, EDS and XRD analyses, the outer layer was composed of γ' and L$_{10}$ martensite, this latter having lattice parameters equal to a = 0.3840 nm and c = 0.3470 nm (c/a = 0.90). The intermediate layer consisted of a continuous γ' layer with a

Table 1
Sample designation and coating fabrication details. In sample name column, A = AM1, P = Pt, PA = Pt + Al and B = β. The asterisk * corresponds to the systems characterized in the as-annealed state (1 cycle of 1 h at 1100 °C) and (d) means default.

Sample Name	Target coating	Fabrication			Pt equivalent thickness (µm)	Al equivalent thickness (µm)
		Electroplating	Heat Treatment	Aluminizing		
A-1* A-2 A-3	Uncoated AM1	–			–	–
P-1 P-2 * P-3	Pt-only γ-γ' 5/0	5 µm	1 h, 1100 °C under vacuum	–	5.2 5.4 5.4	– – –
PA-1 PA-2 PA-3 PA-4 *	Pt + Al γ-γ' 5/2	5 µm		# 1	5.5 5.6 5.5 5.5	2.2 2.1 1.3 1.4
PA-5 PA-6 PA-7 (d) PA-8 *	Pt + Al γ-γ' 5/5	5 µm		# 2	5.2 5.2 5.2 5.6	2.7 2.5 2.2 2.6
PA-9 PA-10 PA-11 *	Pt + Al γ-γ' 7/5	7 µm		# 3	7.0 6.9 6.9	4.5 5.0 4.3
B-1 * B-2 B-3	β-(Ni,Pt)Al	5 µm		APVS	4.9 5.1 4.8	21.8 22.3 22.4

chemical composition close to the objective (Ni-23Al-19Pt-5.6Cr-4.6Co-1.0Ti-1.2Ta-0.9W-1.3Mo in at.%). Similarly to the 5/2 and 5/5 compositions, the inner layer was composed of coarse γ' particles in a γ-matrix. In addition, a number of white precipitates were observed close to the $L_{10} + γ'/γ'$ interface. The EDS analysis indicated that they were rich in tungsten, molybdenum and tantalum. Except for the molybdenum, these γ'-partitioning elements precipitated because they were rejected to the L_{10} phase. Additional white precipitates rich in tungsten, molybdenum, tantalum and chromium were also observed in the superalloy. They corresponded to brittle Topologically-Close-Packed (TCP) phases.

Besides, whatever the Pt + Al γ-γ' composition, many voids were observed at the coating/superalloy interface particularly in the Pt-rich γ' side. The oxide scale characterized by XRD, SEM, Raman spectroscopy and fluorescence contained $α\text{-}Al_2O_3$ and $NiAl_2O_4$ spinel.

As shown in the backscattered image (Fig. 1e), the microstructure of the conventional β-(Ni,Pt)Al coating in the as-annealed condition consisted of a β outer layer above the grit-blasting particles with a lattice parameter of 0.2892 nm. The interdiffusion layer consisted of a 33.1 ± 3.3 µm thick β layer and a4.6 ± 1.2 µm thick γ' layer, both containing a high number of TCP phases. A few secondary reaction zones (SRZ) were also visible at the bond-coating/superalloy interface, which can be detrimental for the mechanical strength [30].

3.2. Oxidation testing

Fig. 2 compares the specimen mass changes of uncoated and coated AM1 systems after cyclic exposure at 1100 °C A magnification is presented in Fig. 2b to better discern the initial mass changes. The oxidation kinetics of all the systems with a Pt + Al γ-γ' coating was rapid during the transient stage which lasted between 10 and 20 cycles at most. Spallation began early, after 400 cycles for few systems but the mass losses were small at each cycle. Based on the first 500 cycles, the Pt + Al γ-γ' coatings exhibited the poorest oxidation performance due to their early spallation. Uncoated AM1 and reference β systems had similar behaviours with parabolic kinetics mainly controlled by the α-

Al_2O_3 growth, as a minor proportion of $NiAl_2O_4$ spinel and $TiTaO_4$ rutile was detected by XRD in both β coated and uncoated superalloy after 500 cycles (Fig. 3). The Pt-only γ-γ' systems showed the longest transient stage and the highest mass gain with no obvious spallation.

After longer exposure, for instance 2000 and 5000 cycles at 1100 °C, the specimen mass change curves evidenced the excellent behaviour of the uncoated AM1. A good behaviour was also obtained for the reference β system when compared with all the Pt-rich γ-γ' systems up to 3000 cycles. Indeed, the mass loss began after 1200 cycles instead of 400 cycles for the Pt + Al γ-γ' systems and 620 cycles for the Pt-only γ-γ'. However, once started, the mass loss of β-(Ni,Pt)Al systems was larger than the one of all Pt-rich γ-γ' coatings. The abrupt slope change can be assimilated to a "breakaway" phenomenon. It was clearly observed after 3800 cycles and can be due to the formation of a new oxide as reported by Littner et al. [31] for β-(Ni,Pt)Al coatings. The specimen mass change of β-(Ni,Pt)Al systems was equal to 0.5 mg/cm² after 1200 cycles and decreased up to -3.4 mg/cm² after 5000 cycles. Finally, it is noted that the Pt-only γ-γ' systems had a higher net mass loss than the one of the Pt + Al γ-γ' systems. After 5500 cycles before increased mass losses compared to 5/5 compositions, the PA-2 sample was removed from the oxidation rig to be characterized. After 10,000 cycles, no catastrophic spallation was observed for the Pt + Al γ-γ' systems. Specimen mass changes of -5.9 mg/cm² and -8.7 mg/cm² were measured for the PA-5 and PA-3 samples, respectively. Catastrophic spallation occurred for PA-1 sample at around 10,500 cycles with an end-of-life reached after 12,655 cycles while PA-6 sample spalled a lot after 12,500 cycles with an end-of-life reached after more than 15,000 cycles.

Based on the mass change curve of a β system tested with another thermal cycling test rig but subjected to the same thermal cycles, the Pt + Al γ-γ' systems had superior cyclic oxidation resistance at 1100 °C than the reference β systems. They outstandingly increased the lifetime of 65% when compared with the β systems. Their catastrophic spallation occurred later and with a less abrupt slope change than for the β systems. However, their early spallation from 400 cycles could be disadvantageous for TBC system applications.

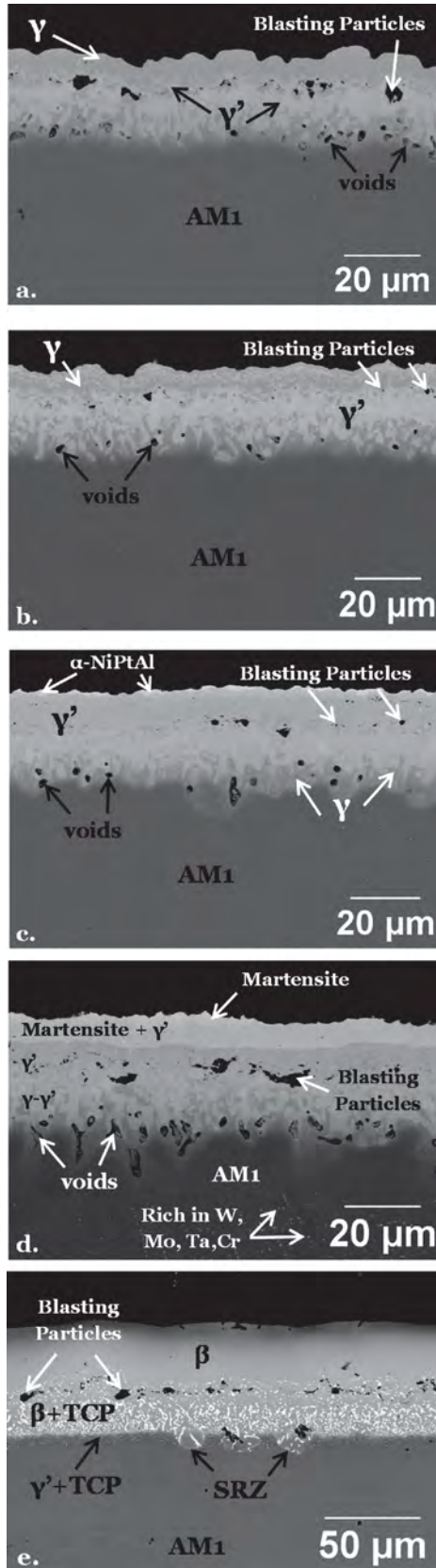**Fig. 1.** Backscattered electron images of cross-sections in the as-annealed state of the systems composed of: (a) a Pt-only γ-γ' coating, (b, c, d) Pt + Al γ-γ' coatings of 5/2, 5/5 and 7/5 compositions respectively and (e) a β-(Ni,Pt)Al coating.

Table 2
Layer thicknesses (µm) of the coatings in the as-fabricated condition.

Coating	Sample ID	Outer layer	Inner layer	Total thickness
Pt-only γ-γ'	P-2	6.0 ± 1.0	17.0 ± 2.0	23.0 ± 2.0
Pt + Al γ-γ' 5/2	PA-4		19.2 ± 2.5	27.2 ± 2.3
Pt + Al γ-γ' 5/5	PA-8	Thin α-NiPtAl layer	17.6 ± 2.3	28.8 ± 2.4
Pt + Al γ-γ' 7/5	PA-11	6.4 ± 1.1	24.2 ± 1.9	
β-(Ni,Pt)Al	B-1	29.5 ± 2.8	37.6 ± 3.3	

Table 3
Average chemical composition (at.%) of the γ-γ' zone in the as-annealed state of the Pt-only γ-γ' bond-coating and the references 5/2 and 5/5 Pt + Al γ-γ' bond-coatings.

Coating	Ni	Al	Pt	Cr	Co	Ti	Ta	W	Mo
Pt only γ-γ' (5/0)	50.4	15.0	19.6	4.0	4.1	1.9	2.7	1.2	1.1
Pt + Al γ-γ' (5/2)	49.1	15.5	15.8	8.2	5.3	1.2	1.8	1.0	2.0
Pt + Al γ-γ' (5/5)	41.7	28.7	13.5	6.4	4.0	1.0	1.9	1.2	1.7
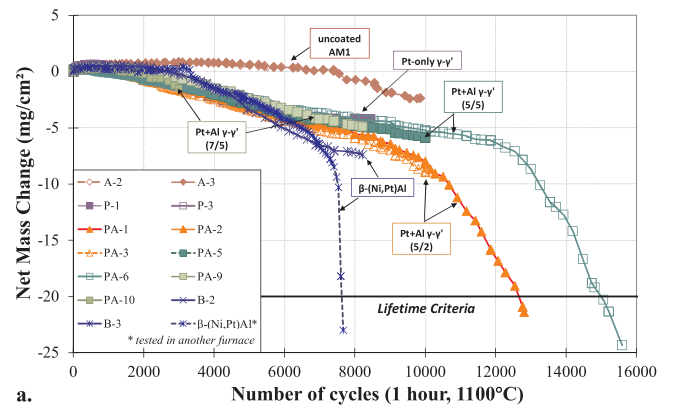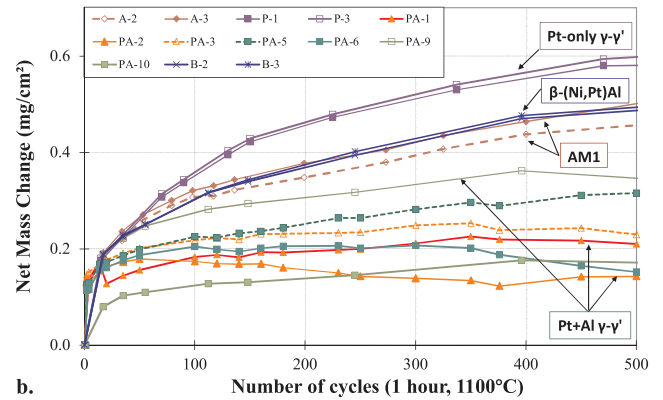
Fig. 2. Net mass changes of coated and uncoated AM1 doped in hafnium during 1 h-cycles at 1100 °C (a) until the end-of-life, (b) after 500 cycles at 1100 °C.

3.3. Kinetics modelling

The p-k_p model [32] was used in order to quantify the cyclic oxidation kinetics previously described. This is a simple statistical model used to fit experimental mass change curves. Based on two parameters, the parabolic constant k_p and the spallation probability p, the model considers the oxidation kinetics as a succession of weight gains by oxidation and mass losses by spallation at the metal/oxide interface [32,33]. One p-k_p value couple was determined for each system after a given number of cycles. However, after very long exposures, some deviations appeared between the experimental and fitted curves when a
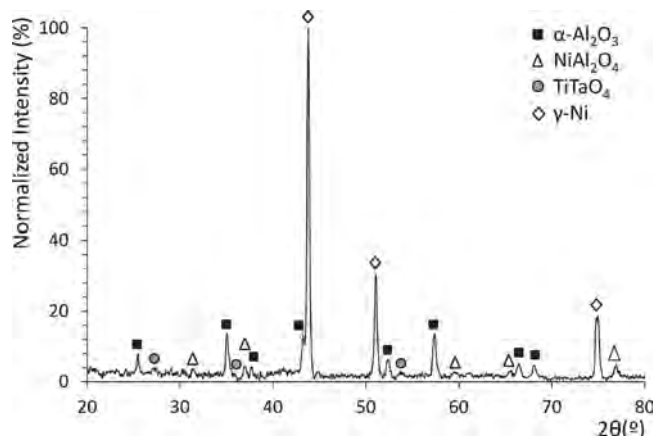
Fig. 3. X-ray diffraction pattern of the uncoated AM1 after 500 cycles at 1100 °C.

single p-k_p couple was applied. Therefore, two or three combinations were used to represent the kinetics which evolve with time. Fig. 4 is an example of a fit based on experimental data of the uncoated Hf-doped AM1 after 6000 cycles at 1100 °C. As illustrated, two successive p-k_p combinations were necessary to reproduce the overall kinetics.

Once the p-k_p couples determined, a p-k_p performance map [32,33] was plotted in order to rank the materials as a function of their resistance to cyclic oxidation. The lower the k_p and p are, the better the resistance to cyclic oxidation is (upper right of the map). In addition, aluminium iso-consumption curves in mg/cm^2 were drawn on the p-k_p maps to easily compare the system performances after a given cycle number [33,34]. When two or more p-k_p combinations were provided, the cycle number corresponding to the kinetics transition was specified close to the arrow indicating the reading direction.

A p-k_p map plotted after 1000 cycles at 1100 °C (Fig. 5a) illustrates the excellent behaviour of the uncoated AM1 with low k_p (9.5×10^{-8} mg^2. cm^{-4}.s^{-1}) and a very low p (0.02%) values. This map also confirmed the good oxidation resistance of the β-(Ni,Pt)Al systems ($k_p = 1.2 \times 10^{-7}$ mg^2. cm^{-4}.s^{-1} and p = 0.04%) when compared with the Pt + Al γ-γ' systems ($k_p = 1.1 \times 10^{-7}$ mg^2. cm^{-4}.s^{-1} and p = 0.12%) and the rapid kinetics of the Pt-only γ-γ' systems with a k_p of 4.2×10^{-7} mg^2. cm^{-4}.s^{-1}. According to the aluminium consumption curve, the Pt-only γ-γ' systems were two or three times less performing (i.e. two or three more Al consumption) than the uncoated AM1 after 1000 cycles at 1100 °C.

After 3000 cycles at 1100 °C (Fig. 5b), the uncoated AM1 still had the best cyclic oxidation resistance in comparison of all coated systems. Pt-only γ-γ' systems and the greater part of Pt + Al γ-γ' systems were in

a steady state cyclic oxidation kinetics regime. Two or three successive p-k_p couples were required to fit the experimental kinetics of the β-(Ni,Pt)Al systems and the Pt + Al γ-γ' with the 7/5 composition evidencing kinetics transitions. Indeed, a kinetic transition appeared at approximately 2200 cycles for the B-2, B-3 and PA-9 samples whereas two kinetics transitions arose after 1200 and 2185 cycles for the PA-10 sample.

After 10,000 cycles, two or three p and k_p combinations were needed to fit the Pt + Al γ-γ' kinetics of the 5/2 and 5/5 systems (Fig. 5c) showing kinetic deviations after 5400 and 6300 cycles. Globally, after the first transition, k_p remained constant and p was increased of about 15–57% depending on the systems. After the second deviation at 6300 cycles, k_p increased of one order of magnitude whereas p decreased of about 50%, as demonstrated by the PA-1 sample.

Besides, the p-k_p model has also the advantage to calculate the average oxide thickness and results can be compared with the experimental ones. Therefore, experimentally, the thickness of the oxide scale of the uncoated AM1 after 5500 cycles was estimated to 6.1 ± 0.7 μm which was consistent with the p-k_p model providing a 6.6 μm thickness. In some cases, the oxide scale was composed of a mixture of Al$_2$O$_3$ and NiAl$_2$O$_4$ spinel, the TiTaO$_4$ fraction being negligible. This mixture can be taken into account in the p-k_p modelling through a factor which converts the mass gain to the consumption of aluminium. The error made when considering that the oxide scale is made only of alumina was estimated to be less than 4%.

3.4. Microstructure after degradation

PA-1 sample of 5/2 composition reached the lifetime criteria after 12,656 cycles at 1100 °C and was removed from the oxidation rig after 12,810 cycles to be characterized while PA-6 sample of 5/5 composition attained the lifetime criteria after 15,000 cycles.

Whatever the number of cycles, the Pt-rich γ-γ' coatings were still composed of the γ and γ' phases. Only the thicknesses of each layer varied with time. The outer layer of the PA-1 system after 12,810 cycles (Fig. 6) with a thickness of 53.1 ± 6.5 μm consisted of a continuous γ layer while the inner part of this coating consisted of a γ-γ' layer of 48.7 ± 17.1 μm thick. A diffusion affected zone of 183.3 ± 16.7 μm was also observed and exhibited γ' rafting.

The chemical compositions of the outer γ and inner γ-γ' layers are reported in Table 3. An average composition of 5.9 at.% of aluminium was still available below the TGO against 12.2 at.% in the γ-γ' zone, this latter being close to the aluminium concentration in the AM1 below the TGO. Platinum concentrations dramatically decreased to reach 1.5 at.% and significant chromium outward diffusion was evidenced with 13 at. %. Titanium and tantalum also diffused outward and concentrations
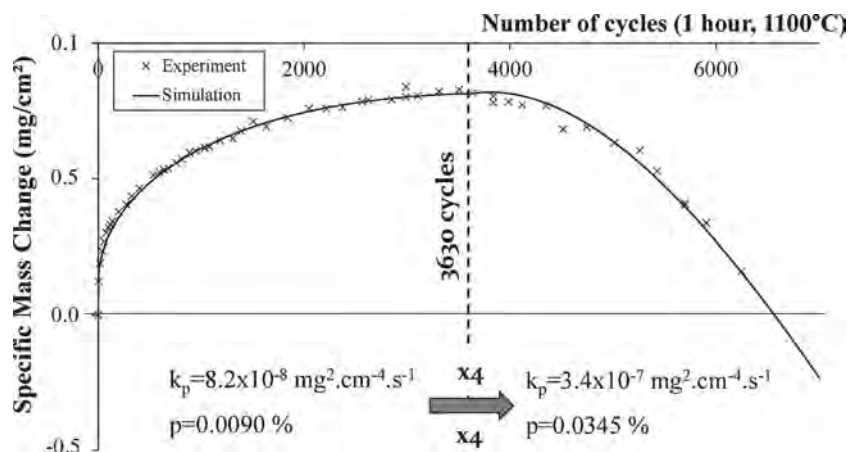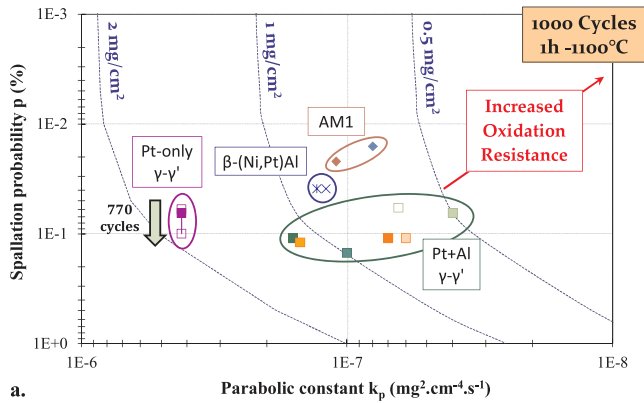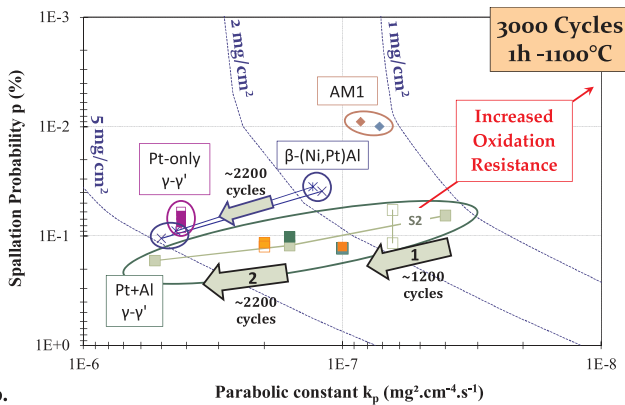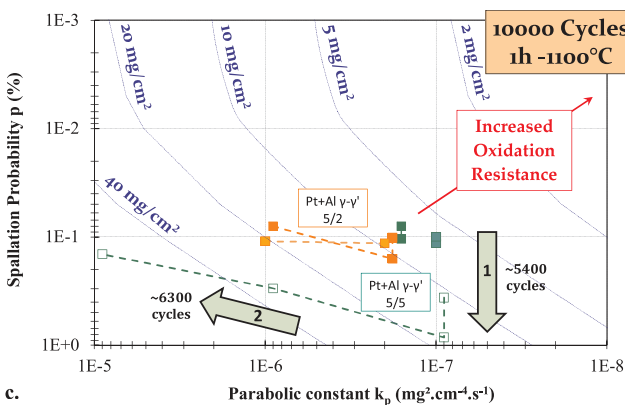

Fig. 4. Example of a model fitting of the experimental data of the uncoated AM1 doped in hafnium after 6000 cycles at 1100 °C.

Fig. 5. "p-k$_p$" map of all the systems (a) after 1000 cycles, (b) after 3000 cycles and (c) after 10,000 cycles for some Pt + Al γ-γ' coatings at 1100 °C.

Fig. 6. SEM-BSE image of the end-of-life microstructure of the Pt + Al γ-γ' coating after 12,810 cycles at 1100 °C (PA-1 sample).

Fig. 7. X-ray diffraction pattern of the Pt + Al γ-γ' coating after 12,810 cycles at 1100 °C (PA-1 sample).

Table 4

Chemical composition (at.%) of the PA-1 sample at the end-of-life after 12,810 cycles at 1100 °C.

Layer	Ni	Al	Pt	Cr	Co	Ti	Ta	W	Mo	Hf
γ	63.6	5.9	1.5	13.0	8.3	1.3	2.3	2.0	2.0	0.1
γ-γ'	65.8	12.2	2.4	5.7	5.4	2.3	4.2	0.6	1.0	0.4

4. Discussion

4.1. Failure mechanisms

According to the specimen mass change curves up to more than 8000 cycles at 1100 °C, the cyclic oxidation resistance of all the systems was ranked as follows:

Uncoated AM1 > Pt + Al γ-γ' > Pt-only γ-γ' > β-(Ni,Pt)Al.

In a general way, oxidation resistance of coated superalloys depends on several criteria. The first one is the aluminium reservoir, i.e. the quantity of aluminium available in the system to maintain a sufficient aluminium concentration below the surface to sustain the growth of the protective α-alumina scale. From this point of view, β-(Ni,Pt)Al are the most promising coatings since they initially contain around 45 at.% of aluminium, i.e. a much higher aluminium quantity than the other systems. The second criteria is the rate of aluminium diffusion towards the metal/oxide interface. This flux of aluminium towards the interface needs to be high enough to sustain alumina growth, and no other less stable oxides. The third criteria is obviously the rate of aluminium

superior to the ones in the AM1 were detected. In addition, a high density of titanium nitrides was observed in the Pt-rich γ outer layer which demonstrated its reduced ability to sustain the growth of alumina over a long time. Indeed, XRD analyses performed after 12,810 cycles revealed that more than 80% of the oxide scale was composed by α-Al$_2$O$_3$ and the remaining 20% consisted of NiAl$_2$O$_4$ and TiTaO$_4$ (Fig. 7). The scale of α-Al$_2$O$_3$ is known to prevent nitrogen ingress in the metal, but this is not the case for the other oxides. Besides, cross sections showed that no void was observed at the interdiffusion zone/substrate interface after long-term exposure at 1100 °C (Table 4).
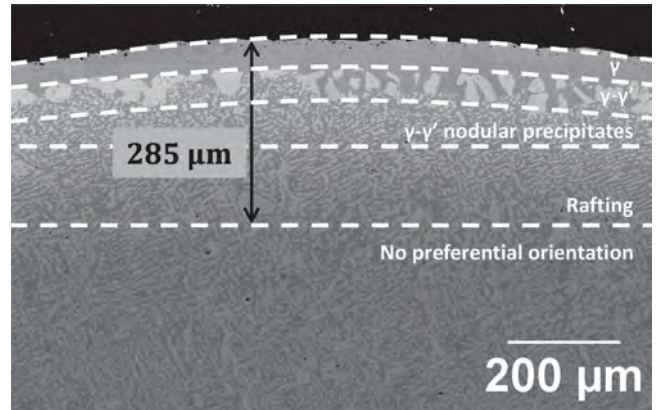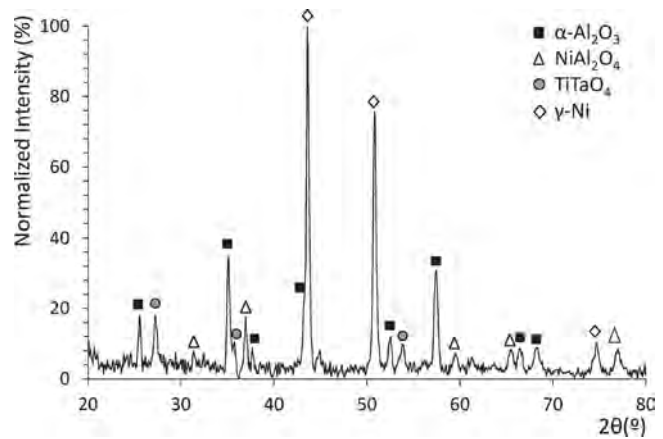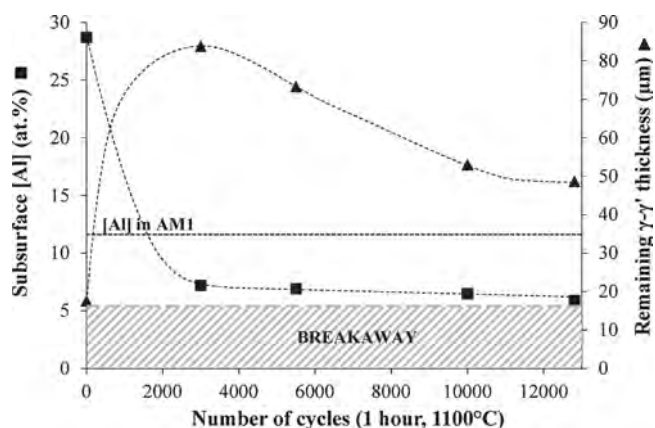
Fig. 8. Evolution with time of the subsurface aluminium concentration (measured by EDX) and the remaining γ-γ' thickness of the Pt + Al γ-γ' coatings.

consumption, which is due to cyclic oxidation at the metal/oxide interface, but also to interdiffusion with the substrate in case of a coating. For example, in this study after 3000 cycles at 1100 °C, a subsurface aluminium concentration of 20 at.% was still available in the β-(Ni,Pt)Al systems whereas 7 at.% was measured in the Pt-rich γ-γ' systems. And as exposure goes along, the "breakaway" of the systems occurs eventually when the aluminium concentration reaches a critical value below the TGO, which is insufficient to sustain the growth of the alumina. In previous studies, this critical aluminium concentration was evaluated to be inferior to 7 at.% in the RT22/CMSX-4 systems [35] and between 6 and 8 at.% in TBC systems containing a Pt-rich γ-γ' coating [36]. Note that with this aluminium level, the alloy just below the oxide scale is all γ-phase. In our case, the critical aluminium content responsible for the breakaway of the Pt-rich γ-γ' systems was estimated at 5.9 at.% in the PA-1 sample after 12,810 cycles, its end-of-life (Fig. 8).

Mechanical aspects are also important to evaluate the protection offered by a coating. Martensitic transformation can take place in the β-(Ni,Pt)Al during thermal cycling. Due to mechanical stresses in the TGO, creep of the coating and the above mentioned martensitic transformation, the β-(Ni,Pt)Al bond-coatings suffer from rumpling [37] and premature catastrophic spallation. At the contrary, the Pt-rich γ-γ' coatings do not suffer from the martensitic transformation, are less affected by rumpling as demonstrated by Selezneff et al. [36] among others [22,35,37,38]. In this study, this was evidenced by a significant mass loss on the specimen mass change curves of β coatings at around 2000 cycles whereas the Pt-rich γ-γ' coatings were much less affected by the surface undulations which was confirmed by the surface and cross-sections observations of the oxide scale. Furthermore, the specimen mass change curves of Pt-rich γ-γ' and β-(Ni,Pt)Al intersected between 4000 and 5000 cycles.

As previously reported [36], the chemical composition of the Pt-rich γ-γ' coatings below the oxide scale seems to be a first-order factor to explain their failure. Firstly, the Pt-only γ-γ' coatings were less performing than Pt + Al γ-γ' coatings. Secondly, by comparing all the Pt + Al γ-γ' coatings despite a small difference in the aluminium content, the greater the initial aluminium content was, the better the resistance was. Although it was difficult to correlate this tendency to the system lifetime, these results confirm that the end-of-life of the Pt-rich γ-γ' systems was induced by a chemical phenomenon ("Chemical Induced Failure") [39]. Therefore, the aluminium addition during fabrication can improve the cyclic oxidation resistance of coated superalloys without top coat. This idea will be compared to the results obtained for complete TBC systems in the part II of this study. It is also noteworthy that the most Pt-rich γ-γ' coatings were fabricated with 5 μm of platinum instead of 7 ± 2 μm, usual platinum thickness for β-(Ni,Pt)Al coatings. On the long term, Pt-rich γ-γ' coatings were superior to β-(Ni,Pt)Al coatings despite a lower content of Pt.

Oxidation and interdiffusion between the coating and the superalloy are responsible for aluminium and platinum depletions in the coating. Both led to the formation of a γ layer below the oxide scale. The presence of this layer was the cause of the end-of-life of the Pt-rich γ-γ' systems. It contributed to the growth of the α-Al₂O₃ scale and to the formation of non-protective oxides as NiAl₂O₄ spinel and TiTaO₄ rutile. The formation of TiTaO₄ at the surface of the alumina scale was the sign of the titanium and tantalum diffusion towards the oxide/gas interface. The presence of the TiTaO₄ oxide can also explain the poorer cyclic oxidation resistance of the Pt-only γ-γ' coatings compared to the Pt + Al γ-γ' coatings which form less TiTaO₄ oxide. A more significant outward diffusion of chromium, titanium and tantalum were evidenced in the Pt-only γ-γ' than in the Pt-rich γ-γ' systems. Moreover, higher Cr, Ti and Ta concentrations than in the AM1 substrate were measured. This implies that platinum favours the uphill diffusion of these three elements, perhaps by decreasing their activity as it is the case for aluminium [29,40]. Therefore, the detrimental effect of titanium and tantalum would be amplified by the higher platinum concentration in Pt-only γ-γ' systems than in Pt + Al γ-γ' systems. It is also important to note that no nickel oxide NiO was detected at the end-of-life. Thus, the aluminium concentration below the TGO of 5.9 at.% was sufficient to prevent its formation and to favour the spinel NiAl₂O₄.

As previously mentioned, the breakaway of the alumina-forming nickel based superalloys is characterized by an acceleration of the mass loss which can be related to the formation of a new oxide [31]. The p-k_p modelling showed that a unique combination of p and k_p was not sufficient to fit the cyclic oxidation kinetics between the entire 0 and 10,000 cycles interval at 1100 °C. Depending on the kinetics, two or three combinations were required. By comparing the first and the second p and k_p combination of the Pt + Al γ-γ' coatings, the k_p remained constant but the p increased by a factor 2. Then between the second and the third combination, the k_p increased by a factor 10 at each slope change and the p afresh decreased by a factor 2 (Fig. 5). Consistently with XRD analyses, the k_p remains approximately constant and typical of α-alumina growth as long as this oxide form a continuous and protective oxide scale. At the same time, the parameter "p" may increase because of changes in the stress state of the interface due to rumpling and because of segregations at the oxide/scale interface which may affect the oxide adhesion. If spallation becomes more pronounced, for a given and constant k_p, then, the rate of Al consumption increases. Therefore, a breakaway can occur locally with the formation of a fast-growing oxide which in turns increases the k_p. As the k_p of a spinel is 10–100 times higher than the one of α-Al₂O₃, only a small proportion of spinel in the oxide scale is necessary to explain the observed k_p evolution. However, no difference in the spinel proportion was detected with XRD analyses.

4.2. Aluminium effect

The end-of-life of the Pt-rich γ-γ' coatings is directly linked to their chemical composition. The content of the protective element, in this case aluminium, is a first-order factor for the lifetime. According to the specimen mass change curves, aluminium addition during the fabrication of the Pt-rich γ-γ' coatings enhanced the lifetime. Even though the end-of-life of the Pt-only γ-γ' coatings was not reached, the Pt + Al γ-γ' coatings were more resistant after 6000 cycles at 1100 °C when compared with systems without the short-term aluminizing.

The quantity of aluminium consumption by oxidation was determined by the p-k_p model and plotted versus the number of cycles (Fig. 9). The aluminium consumption obviously depended on the p-k_p combinations used to adjust the experimental data. For relatively short durations when compared with the industrial application, the aluminium quantity deposited during fabrication did not affect the cyclic oxidation resistance. This was consistent with the p-k_p maps after 1000 cycles at 1100 °C showing that all the Pt + Al γ-γ' systems had similar p and k_p values (Fig. 5a). But for longer exposures, an influence was
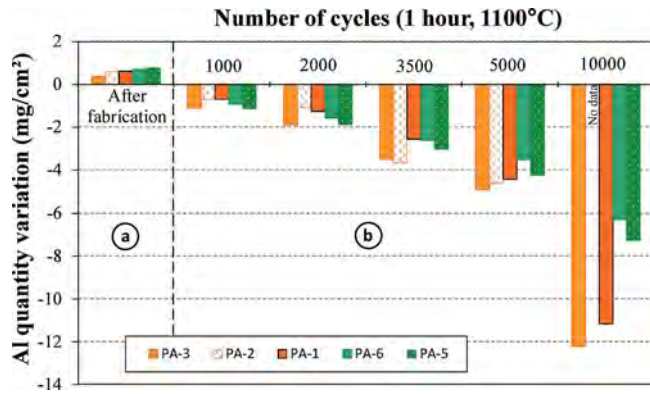
Fig. 9. (a) Al mass gain after aluminizing, (b) evolution with time of the calculated Al consumption of some Pt + Al γ-γ' coatings, according to the "p-k$_p$" model.

noticed (Fig. 5b and c). The greater the aluminium quantity deposited during the short-term aluminizing was, the less the aluminium consumption was. After 10,000 cycles, an aluminium loss of - 12.2 mg/cm^2 was estimated for the PA-3 sample enriched with 1.3 µm of aluminium against a loss of - 6.3 mg/cm^2 for the PA-6 sample with the addition of 2.5 µm of aluminium. This confirmed that aluminium addition during the coating fabrication decreased the cyclic oxidation kinetics and delayed the breakaway.

4.3. AM1 superalloy behaviour

As demonstrated by the specimen mass changes and the p-k$_p$ modelling, the Pt-rich γ-γ' bond-coating did not enhance the cyclic oxidation resistance of the new AM1 doped in hafnium after 10,000 cycles at 1100 °C. After 5500 cycles, the microstructure of the uncoated AM1 consisted of three distinct layers (Fig. 10): (i) a γ outer layer of 11.8 ± 5.6 µm thick, (ii) a γ-γ' inner layer of 67.8 ± 11.7 µm thick containing coarse γ' grains and (iii) a diffusion-affected zone containing cuboids γ' precipitates and γ' rafting in a γ matrix. This corresponded to the microstructural features observed for the Pt + Al γ-γ' systems after the same duration although platinum was absent. Nevertheless, the slightly thinner γ outer layer in the AM1 systems attested to a smaller
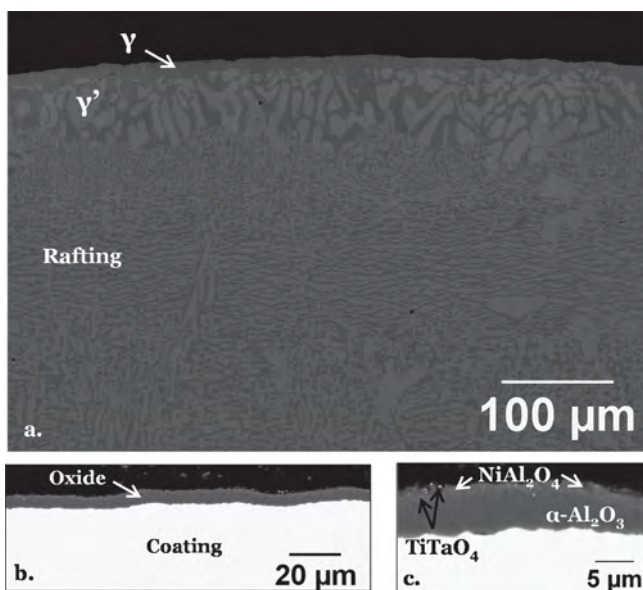

Fig. 10. Backscattered electron images of metallographic cross-section of the uncoated AM1 doped in hafnium after 5500 cycles at 1100 °C: (a) general overview of the superalloy, (b, c) fully-adherent oxide scale.

aluminium depletion due to its slower oxidation kinetics. EDS analyses confirmed the lower depletion by indicating an aluminium concentration of 10.8 ± 0.8 at.% in the large γ' grains which was higher than the one in the Pt + Al γ-γ' systems (9.2 ± 0.3 at;%) after 5500 cycles at 1100 °C.

The oxide scale observations did not allow to understand the different kinetics between coated and uncoated systems. Indeed, the oxide scale was perfectly adherent on the AM1 system after 5500 cycles at 1100 °C. According to the XRD analyses, it was composed of the same oxides than previously, α-Al$_2$O$_3$, NiAl$_2$O$_4$ and TiTaO$_4$. No hafnium oxide was detected by SEM-EDX neither in the oxide scale nor at the metal/oxide interface. However a very low amount of Hf (thin atomic layer) at the metal/oxide interface and at the grain boundaries can be sufficient to slow down both the growth and the spallation kinetics and explain the excellent behaviour of the uncoated AM1.

The p-k$_p$ model shows that two combinations of p and k$_p$ were required to well reproduce the kinetics of the AM1 after 6000 cycles at 1100 °C. A slope variation appeared at around 3630 cycles. After 6000 cycles, both the k$_p$ and p increased by a factor 4 suggesting that breakaway was initiated with the formation of a faster growing and faster spalling oxide.

AM1 superalloy doped with Hf was superior to β and γ-γ' coatings during thermal cycling at 1100 °C. Nevertheless, all the systems behaved well with relatively low oxidation and spallation kinetics. The superiority of uncoated AM1 superalloy was consistent and most likely due to the Hf doping which reduces slightly the oxidation kinetics and decreases alumina scale spallation. Indeed, the same alloy without Hf doping behaved not as good [41]. This means that there is perhaps room for coating improvement through a Hf doping of the coatings themselves or through a higher Hf doping of the substrate which would lead to a higher level of Hf in the γ-γ' coatings.

Also, it is necessary to state here that this superiority of the uncoated AM1 superalloy does not mean that the coatings are not necessary. Indeed, the superalloy also needs to be a good alumina former at lower temperatures, which is not obvious due to its lower level of Al. Secondly, coatings are useful for protection against high temperature corrosion in presence of SO$_2$ and NaCl. Thirdly, cyclic oxidation tests of AM1/YSZ systems without bond-coating could be necessary to fully evaluate the bond-coating efficiency.

5. Conclusion

The aim of this study was to study the oxidation behaviour of Pt-rich γ-γ' bond-coatings fabricated by using conventional industrial processes. The cyclic oxidation kinetics at 1100 °C were determined experimentally over very long durations and were quantified by using the p-k$_p$ model in order to compare the coated and uncoated systems. The p-k$_p$ maps highlighted the excellent behaviour of the uncoated AM1 first generation superalloy doped in hafnium up to at least 6000 cycles of 1 h at 1100 °C. Its outstanding performance can be attributed to the optimization of the hafnium doping and the low sulphur content despite its high titanium concentration. In addition, it was shown that the Pt-rich γ-γ' bond-coatings on AM1 showed a better cyclic oxidation resistance at 1100 °C than the reference system with a β-(Ni,Pt)Al coating. Among the Pt-rich γ-γ' bond-coatings, a better resistance was observed for the Pt + Al γ-γ' coatings prepared from a platinum electroplating and a "short-term" aluminizing step when compared with the Pt-only γ-γ' coatings after 8000 cycles of 1 h at 1100 °C. Aluminium addition during fabrication of γ-γ' coatings improved the cyclic oxidation performance of coated AM1 systems. Besides, it seems that Al addition in the Pt γ-γ' coatings decreases the detrimental effect of titanium and tantalum by decreasing their segregation in the γ' phase close to the surface which otherwise led to the TiTaO$_4$ formation.

The breakaway of the Pt-rich γ-γ' coatings was a rapid mass loss due to an insufficient aluminium content below the TGO whereas the reference β-(Ni,Pt)Al system suffered from rumpling. However, at the

end-of-life, γ subsurface layer still exhibited relative good oxidation properties since no NiO was identified in the oxide scale (only α-Al$_2$O$_3$, NiAl$_2$O$_4$ and TiTaO$_4$ were seen) but nitrides were observed below the scale.

Acknowledgements

References

[1] J.A. Haynes, B.A. Pint, Y. Zhang, I.G. Wright, Comparison of the Oxidation Behavior of [beta] and [gamma]-[gamma]' NiPtAl Coatings, Surf. Coat. Technol. 204 (2009) 816–819.

[2] A. Nagaraj, W.B. Connor, R.W. Jendrix, D.J. Wortman, L.W. Plemmons, Platinum, Rhodium, or Palladium Protective Coatings in Thermal Barrier Coatingg Systems, G.E. Company, United States, 1995.

[3] D.S. Rickerby, S.R. Bell, R.G. Wing, Method of Applying a Thermal Barrier Coating to a Superalloy Article and a Thermal Barrier Coating, (1997) United States.

[4] K. Bouhanek, O.A. Adesanya, F.H. Stott, P. Skeldon, D.G. Lees, G.C. Wood, High temperature oxidation of thermal barrier coating systems on RR3000 substrates: Pt Aluminide bond coats, Mater. Sci. Forum 639 (2001) 369.

[5] R. Swadźba, J. Wiedermann, L. Swadźba, M. Hetmańczyk, B. Witala, U. Schulz, T. Jung, High temperature oxidation of EB-PVD TBCs on Pt-diffused single crystal Ni superalloy, Surf. Coat. Technol. 260 (2014) 2–8.

[6] H.M. Tawancy, A.I. Mohamed, N.M. Abbas, R.E. Jones, D.S. Rickerby, Effect of superalloy substrate composition on the performance of a thermal barrier coating system, J. Mater. Sci. 38 (2003) 3797–3807.

[7] J.A. Haynes, B.A. Pint, Y. Zhang, I.G. Wright, Comparison of the cyclic oxidation behavior of β-NiAl, β-NiPtAl and γ-γ' NiPtAl coatings on various superalloys, Surf. Coat. Technol. 202 (2007) 730.

[8] R.T. Wu, K. Kawagishi, H. Harada, R.C. Reed, The retention of thermal barrier coating systems on single-crystal superalloys: Effects of substrate composition, Acta Mater. 56 (2008) 3622–3629.

[9] H.M. Tawancy, A.I. Mohammad, L.M. Al-Hadhrami, H. Dafalla, F.K. Alyousf, On the performance and failure mechanism of thermal barrier coating systems used in gas turbine blade applications: Influence of bond coat/superalloy combination, Eng. Fail. Anal. 57 (2015) 1–20.

[10] D.P. Whittle, J. Stringer, Improvements in high temperature oxidation resistance by additions of reactive elements or oxide dispersions, Philos. Trans. R. Soc. London A295 (1980) 309.

[11] B.A. Pint, I. Wright, W. Lee, Y. Zhang, K. Prübner, K. Alexander, Substrate and bond coat compositions: factors affecting alumina scale adhesion, Mater. Sci. Eng. A A245 (1998) 201–211.

[12] B.A. Pint, J.H. Schneibel, The effect of carbon and reactive element dopants on oxidation lifetime of FeAl, Scr. Mater. 52 (12) (2005) 1199–1204.

[13] P.Y. Hou, T. Izumi, B. Gleeson, Sulfur Segregation at Al2O3/gamma-Ni +gamma'-Ni3Al Interfaces: Effects of Pt, Cr and Hf Additions, Oxid. Met. (2009) 109–124.

[14] B. Gleeson, W. Wang, S. Hayashi, D. Sordelet, Effects of Platinum on the Interdiffusion and oxidation Behavior of Ni-Al-Based Alloys, Mater. Sci. Forum 461–464 (2004) 213–222.

[15] B. Sundman, S. Ford, X.G. Lu, T. Narita, D. Monceau, Experimental and simulation study of uphill diffusion of Al in a Pt-Coated gamma-Ni-Al model alloy, J. Phase Equilibria Diffus. (2009) 602–607.

[16] P. Audigié, A. Rouaix-Vande Put, A. Malié, P. Bilhé, S. Hamadi, D. Monceau, Observation and modeling of alpha-NiPtAl and Kirkendall void formations during interdiffusion of a Pt coating with a gamma-(Ni-13Al) alloy at high temperature, Surf. Coat. Technol. 260 (2014) 9–16.

[17] J.A. Haynes, Y. Zhang, W.Y. Lee, B.A. Pint, I.G. Wright, K.M. Cooley, Effects of platinum additions and sulfur impurities on the microstructure and scale adhesion behavior of single-phase CVD aluminide bond coat, Elevated Temperature Coatings : Science and Technology III, The Minerals, Metals and Materials Society, 1999.

[18] B.A. Pint, J.A. Haynes, K.L. More, I.G. Wright, C. Leyens, Compositional effects on aluminide oxidation performance: objectives for improved bond coats, Superalloys, TMS, Warrendale, PA, 2000.

[19] Y. Cadoret, D. Monceau, M. Bacos, P. Josso, V. Maurice, P. Marcus, Effect of platinum on the growth rate of the oxide scale formed on cast nickel aluminide intermetallic alloys, Oxid. Met. 64 (3–4) (2005) 185–205.

[20] Y. Zhang, J.A. Haynes, W.Y. Lee, I.G. Wright, B.A. Pint, K.M. Cooley, P.K. Liaw, Effects of Pt incorporation on the isothermal oxidation behavior of CVD aluminide coatings, Metallurgical and materials Transaction A 32A (2001) 1727–1741.

[21] Y. Cadoret, M.-P. Bacos, P. Josso, V. Maurice, P. Marcus, S. Zanna, Study of the sulfur segregation on Pt-modified Nickel Aluminides and its influence on the TBC spallation mechanism, Mater. Sci. Forum (2004).

[22] R.T. Wu, X. Wang, A. Atkinson, On the interfacial degradation mechanisms of thermal barrier coating systems: Effects of bond coat composition, Acta Mater. 58 (17) (2010) 5578–5585.

[23] C. Jiang, B. Gleeson, Site preference of transition metal elements in Ni3Al, Scr. Mater. (2006) 433–436.

[24] C. Jiang, B. Gleeson, Surface segregation of Pt in [gamma]'-Ni3Al: a first-principles study, Acta Mater. (2007) 1641–1647.

[25] F. Qin, C. Jiang, J.W. Anderegg, C.J. Jenks, B. Gleeson, D.J. Sordelet, P.A. Thiel, Segregation of Pt at clean surfaces of (Pt, Ni)(3)Al, Surf. Sci. (2007) 376–380.

[26] B. Gleeson, N. Mu, S. Hayashi, Compositional factors affecting the establishment and maintenance of Al2O3 scales on Ni–Al–Pt systems, J. Mater. Sci. (2009) 1704–1710.

[27] S. Selezneff, Etude et développement de revêtements γ-γ' riches en platine, élaborés par Spark Plasma Sintering (SPS). Application au système barrière thermique, PhD Thesis Institut National Polytechnique de Toulouse, France, 2011.

[28] D. Monceau, D. Oquab, C. Estournes, M. Boidot, S. Selezneff, Y. Thebault, Y. Cadoret, Pt-modified Ni aluminides, MCrAlY-base multilayer coatings and TBC systems fabricated by Spark Plasma Sintering for the protection of Ni-base superalloys, Surf. Coat. Technol. 204 (6–7) (2009) 771–778.

[29] P. Audigié, Modélisation de l'interdiffusion et du comportement en oxydation cyclique de superalliages monocristallins à base de nickel revêtus d'une sous-couche γ-γ' riche en platine. Extension aux systèmes barrière thermique, PhD Thesis Institut National Polytechnique de Toulouse, France, 2015.

[30] Y. Matsuoka, Y. Aoki, K. Matsumoto, T. Suzuki, K. Chikugo, K. Murakami, et al., The formation of SRZ on a fourth generation single crystal superalloy applied on with aluminide coating, in: K.A. Green (Ed.), Superalloys, TMS, Warrendale, PA, 2004, pp. 637–642.

[31] A. Littner, M. Schütze, The cyclic oxidation behaviour of several aluminide and platinum aluminide diffusion coatings at 1150°C, Corrosion Science in the 21st Century, (2003).

[32] D. Poquillon, D. Monceau, Application of a simple statistical spalling model for the analysis of high temperature, cyclic oxidation kinetics data, Oxid. Met. 59 (3–4) (2003) 409–431.

[33] D. Poquillon, D. Monceau, et al., Prediction of high temperature cyclic oxidation kinetics with simple statistical spalling model, in: P.K. Liaw, R.A. Buchanan, D.L. Klarstrom (Eds.), Symposium on Materials Lifetime Science and Engineering Held at the 2003 TMS Annual Meeting (2003) 165–172.

[34] N. Vialas, D. Monceau, B. Pieraggi, Effect of cycle frequency on high temperature oxidation behavior of alumina-forming coatings used for industrial gas turbine blades, High Temperature Corrosion and Protection of Materials 6, Prt 1 and 2, Proceedings (2004) 747–754.

[35] N. Vialas, Etude de la détérioration par oxydation haute température et interdiffusion des systèmes revêtement/superalliage à base de nickel. Prévision de la durée de vie, PhD Thesis Institut National Polytechnique de Toulouse, France, 2004.

[36] S. Selezneff, M. Boidot, J. Hugot, D. Oquab, C. Estournès, D. Monceau, Thermal cycling behavior of EBPVD TBC systems deposited on doped Pt-rich gamma-gamma prime bond coatings made by Spark Plasma Sintering (SPS), Surf. Coat. Technol. 206 (2011) 1558–1565.

[37] D.S. Balint, T. Xu, J.W. Hutchinson, A.G. Evans, Influence of bond coat thickness on the cyclic rumpling of thermally grown oxides, Acta Mater. 54 (7) (2006) 1815–1820.

[38] T. Izumi, N. Mu, L. Zhang, B. Gleeson, Effects of targeted γ-Ni + γ'-Ni3Al-based coating compositions on oxidation behavior, Surf. Coat. Technol. 202 (2007) 628–631.

[39] H.E. Evans, Oxidation failure of tbc systems: an assessment of mechanisms, Surface and Coatings Technology, (2011) In Press, Accepted Manuscript.

[40] A. Vande Put, D. Oquab, E. Péré, A. Raffaitin, D. Monceau, Beneficial Effect of Pt and of Pre-Oxidation on the Oxidation Behaviour of an NiCoCrAlYTa Bond-Coating for Thermal Barrier Coating Systems, Oxid. Met. 75 (5) (2011) 247–279.

[41] E. Fedorova, D. Monceau, D. Oquab, Quantification of growth kinetics and adherence of oxide scales formed on Ni-based superalloys at high temperature, Corros. Sci. (2010) 3932–3942.